Influence of Substituents on Cation−π Interactions. 2. Absolute Binding Energies of Alkali Metal Cation−Fluorobenzene Complexes Determined by Threshold Collision-Induced Dissociation and Theoretical Studies

R. Amunugama and M. T. Rodgers*

Department of Chemistry, Wayne State University, Detroit, Michigan 48202

Received: February 19, 2002; In Final Form: May 29, 2002

Threshold collision-induced dissociation of $M^+(C_6H_5F)$ and $M^+(C_6H_5F)_2$ with Xe is studied by guided ion beam mass spectrometry. M^+ include the following alkali metal ions: Li^+, Na^+, K^+, Rb^+, and Cs^+. In all cases, the primary and lowest energy dissociation channel observed is endothermic loss of an intact fluorobenzene ligand. Sequential dissociation of a second fluorobenzene ligand is observed at elevated energies in the bis complexes. Minor production of ligand exchange products, M^+Xe and $M^+(C_6H_5F)Xe$, is also observed. The cross section thresholds for the primary dissociation channel are interpreted to yield 0 and 298 K bond dissociation energies for $(C_6H_5F)_{x-1}M^+-C_6H_5F$, $x = 1$ and 2, after accounting for the effects of multiple ion−neutral collisions, the kinetic and internal energies of the reactants, and dissociation lifetimes. Density functional theory calculations at the B3LYP/6-31G* level of theory are used to determine the structures of these complexes and provide molecular constants necessary for the thermodynamic analysis of the experimental data. Theoretical binding energies are determined from single-point energy calculations at the MP2(full)/6-311+G(2d,2p) level using the B3LYP/6-31G* geometries. Zero-point energy and basis-set superposition error corrections are also included. The agreement between theory and experiment is very good when full electron correlation is included (for Li^+, Na^+, and K^+), except for the $Li^+(C_6H_5F)$ complex, and reasonable when effective core potentials are used (for Rb^+ and Cs^+). The trends in $M^+(C_6H_5F)_x$ binding energies are explained in terms of varying magnitudes of electrostatic interactions and ligand−ligand repulsion in the complexes. Comparisons are also made to previous theoretical and experimental BDEs of $M^+(C_6H_6)_x$ and $M^+(C_6H_5CH_3)_x$ to examine the influence of the fluoro substituent on the binding and the factors that control the strength of cation−π interactions.

Introduction

Recently, there has been a growing interest in a specific noncovalent interaction, the cation−π interaction, and its role in molecular recognition in biological systems. Comprehensive reviews of cation−π interactions by Dougherty and co-workers[1,2] provide a detailed overview of cation−π interactions, highlighting both the fundamental nature of such interactions and their biological importance. The pioneering experimental work by Kebarle and co-workers[3] showed that the noncovalent interaction of K^+ with benzene, a nonpolar molecule, was significant and stronger than the interaction of K^+ with a single water molecule. It is believed that cation−π interactions play an important role in protein structural organization[1,2,4−8] and the functioning of ionic channels in membranes.[9,10] In addition, a number of studies have established that cation−aromatic interactions are very important in protein−ligand interactions, as well.[1] Statistical analyses of the crystal structures of a variety of proteins showed that the nitrogen atoms in the side chains of arginine, lysine, asparagine, glutamine, and histidine preferentially position themselves close to the aromatic residues of phenylalanine, tyrosine, and tryptophan.[11,12] It was also found that energetically significant cation−π interactions are common in proteins and that they probably contribute to protein stability. Certain favorable cation−π interaction pairs contribute at least as much to protein stability and the structural profile of a native protein as do more conventional noncovalent interactions. Hence, cation−π interactions are now considered as important as hydrogen bonds, salt bridges, and hydrophobic effects in analyses of the stability of native protein structure.[12] Cation−π interactions operative in biological systems may involve monovalent or divalent atomic metal ions or may involve closed-shell nonmetallic molecular cations such as alkylammonium ions.[1,2,13] Of the alkali metal ions, cation−π complexes involving Na^+ and K^+ are the most biologically relevant.[14] An example of experimental evidence for cation−π interactions in proteins is observed in the crystal structure of hen egg-white lysozyme.[15] In this protein, the cation−π interaction is between Na^+ and the indole side chain of tryptophan (residue Trp 123). The distance between the center of the indole ring of Trp123 and Na^+ is 4.07 Å. Systems involving the larger alkali metal cations, Rb^+ and Cs^+, have thus far received much less attention. However, Cs^+ is reported to have been useful in protein crystal structure determinations,[13] where it is believed to coordinate with aromatic residues through cation−π interactions. Thus, the importance of understanding cation−π interactions involving alkali metal ions, both from a fundamental perspective and the detailed role that they play in biological systems, is obvious.

To gain a better understanding of the interaction of alkali metal ions with large biological molecules, knowledge of the structure and energetics of binding to smaller model systems is required. Furthermore, characterizing these interactions in the gas phase is an important and essential part of building a

* To whom correspondence should be addressed.

10.1021/jp020459a CCC: $22.00
Published on Web 08/13/2002

database of information concerning the nature and strength of cation−π interactions and the influence of the local environment on such interactions. A number of model systems[3,16−24] as well as the aromatic amino acids,[25,26] in which the neutral ligand binds through its π electrons, have been studied in the gas phase. Among the model systems examined, benzene[3,16−20] and pyrrole,[21,22] and their derivatives such as toluene,[24] phenol, and indole,[23] are of particular interest. These model systems constitute the simplest groups of larger aromatic ligands that mimic the binding properties of π-donating ligands believed to participate in cation−π interactions operative in biological systems. Complementary to the gas-phase experimental studies are high-level theoretical calculations, which have been performed for several of the above systems at various levels of theory.[1,21−24,27,28]

In an effort aimed at understanding the influence of substituents on cation−π interactions, we set out to determine the absolute binding energies of alkali metal cations to several substituted benzene complexes. In this series of studies, we first examined the influence of a methyl substituent.[24] In this case, toluene is actually a better model system than benzene for the study of cation−π interactions operative in biological systems because the side chain of each of the aromatic amino acids has a methylene group attached to the aromatic ring. In the present study, we examine the influence of a fluoro substituent by examining cation−π interactions between the alkali metal ions (Li^+, Na^+, K^+, Rb^+, and Cs^+) and fluorobenzene. Although fluorobenzene is not of direct biological interest, fluorinated benzenes are found in the skeleton of some inhibitors[29] and certain antibiotic drugs such as Ciprofloxacin (cipro), which is used for treatment of inhalation anthrax exposure.[30] There have been several experimental and theoretical studies on the interactions of Na^+,[31] Cr^+,[32,33] Fe^+,[33,34] Co^+,[33] and Au^+ and Au^- [35] complexed to fluoro-substituted benzenes and toluenes. Of the substituted flurobenzenes studied, 1,3,5-trifluorobenzene is of particular interest in the study of influence of the quadrupole moment on the strength of the cation−π interaction, because it is known to possess a nearly zero quadrupole moment. However, experimental studies on alkali metal cation−π interactions with fluorobenzene have not been reported in the literature.

In recent work, we have developed methods to allow the application of quantitative threshold collision-induced dissociation (CID) methods to obtain accurate thermodynamic information on increasingly large systems.[19,22,24,36−51] One of the driving forces behind these developments is our interest in applying such techniques to systems having biological relevance. In addition, we seek to perform accurate thermochemical measurements that provide absolute anchors for metal cation affinity scales over an ever-broadening range of energies and molecular systems. In the present paper, we examine cation−π interactions of fluorobenzene, C_6H_5F, with the alkali metal ions Li^+, Na^+, K^+, Rb^+, and Cs^+. The structure of fluorobenzene along with its measured[52] and calculated dipole moments (determined here) and estimated polarizability[53] are shown in Figure 1. The kinetic energy-dependent cross sections for the primary CID process observed in each system are analyzed by methods developed previously.[40] The analysis explicitly includes the effects of the internal and translational energy distributions of the reactants, multiple ion−neutral collisions, and the lifetime for dissociation. We derive $(C_6H_5F)_{x-1}M^+-C_6H_5F$, $x = 1$ and 2, bond dissociation energies (BDEs) for all of the complexes and compare these results to ab initio and density functional calculations performed here and in the literature.[31] Comparisons are also made to the analogous benzene[20] and toluene[24] systems studied previously to examine the influence of the fluoro substituent on the binding and the factors that control the strength of cation−π interactions. Finally, comparisons are made to other fluoro-substituted benzenes and toluenes binding to a variety of metal ions.[33,34]

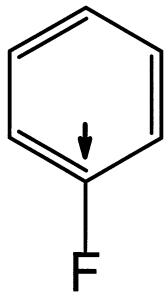

Fluorobenzene
1.60 D (1.91 D)
9.86 Å^3

Figure 1. Structure of the fluorobenzene molecule. The properly scaled dipole moment is shown as an arrow. Values listed are taken from experiment[46] and theoretical calculations performed here (in parentheses). The estimated polarizability is also shown.[47]

Experimental Section

General Procedures. Cross sections for collision-induced dissociation of $M^+(C_6H_5F)_x$ complexes, where $x = 1$ and 2 and $M^+ = Li^+$, Na^+, K^+, Rb^+, and Cs^+, are measured using a guided ion beam mass spectrometer that has been described in detail previously.[45] The $M^+(C_6H_5F)_x$ complexes are generated in a flow tube ion source by condensation of the alkali metal ion and neutral fluorobenzene molecule(s). These complexes are collisionally stabilized and thermalized by $\sim 10^5$ collisions with the He and Ar bath gases such that the internal energies of the ions emanating from the source region are well described by a Maxwell−Boltzmann distribution at room temperature.[45] The ions are extracted from the source, accelerated, and focused into a magnetic sector momentum analyzer for mass analysis. Mass-selected ions are decelerated to a desired kinetic energy and focused into an octopole ion guide, which traps the ions in the radial direction.[54] The octopole passes through a static gas cell containing Xe, used as the collision gas, for reasons described elsewhere.[55−57] Low gas pressures in the cell (typically 0.05−0.20 mTorr) are used to ensure that multiple ion−neutral collisions are improbable. Product and unreacted beam ions drift to the end of the octopole where they are focused into a quadrupole mass filter for mass analysis and subsequently detected with a secondary electron scintillation detector and standard pulse counting techniques.

Ion intensities are converted to absolute cross sections as described previously.[58] Absolute uncertainties in cross section magnitudes are estimated to be ±20%, which are largely the result of errors in the pressure measurement and the length of the interaction region. Relative uncertainties are approximately ±5%. Because the radio frequency used for the octopole does not trap light masses with high efficiency, the cross sections for Li^+ products were more scattered and showed more variations in magnitude than is typical for heavier ions.

Therefore, absolute magnitudes of the cross sections for production of Li^+ are probably accurate to ±50%.

Ion kinetic energies in the laboratory frame, E_{lab}, are converted to energies in the center of mass frame, E_{CM}, by the formula $E_{CM} = E_{lab}\, m/(m+M)$, where M and m are the masses of the ionic and neutral reactants, respectively. All energies reported below are in the CM frame unless otherwise noted. The absolute zero and distribution of the ion kinetic energies are determined using the octopole ion guide as a retarding potential analyzer as previously described.[58] The distribution of ion kinetic energies is nearly Gaussian with a full width at half-maximum (fwhm) typically between 0.2 and 0.4 eV (lab) for these experiments. The uncertainty in the absolute energy scale is ±0.05 eV (lab).

Even when the pressure of the reactant neutral is low, it has previously been demonstrated that the effects of multiple collisions can significantly influence the shape of CID cross sections.[59] We have performed pressure-dependent studies of all cross sections examined here. In the present systems, we observe small cross sections at low energies that have an obvious dependence upon pressure. We attribute this to multiple energizing collisions that lead to an enhanced probability of dissociation below threshold as a result of the longer residence time of these slower moving ions. Data free from pressure effects are obtained by extrapolating to zero reactant pressure, as described previously.[59] Thus, results reported below are due to single bimolecular encounters.

Thermochemical Analysis. The threshold regions of the reaction cross sections are modeled using eq 1,

$$\sigma(E) = \sigma_0 \sum_i g_i (E + E_i - E_0)^n / E \qquad (1)$$

where σ_0 is an energy-independent scaling factor, E is the relative translational energy of the reactants, E_0 is the threshold for reaction of the ground electronic and rovibrational state, and n is an adjustable parameter. The summation is over the rovibrational states of the reactant ions, i, where E_i is the excitation energy of each rovibrational state and g_i is the population of those states ($\Sigma g_i = 1$). The populations of excited rovibrational levels are not negligible even at 298 K as a result of the many low-frequency modes present in these ions. The relative reactivity of all rovibrational states, as reflected by σ_0 and n, is assumed to be equivalent.

The Beyer−Swinehart algorithm[60] is used to evaluate the density of the rovibrational states, and the relative populations, g_i, are calculated by an appropriate Maxwell−Boltzmann distribution at the 298 K temperature appropriate for the reactants. The vibrational frequencies of the reactant complexes are determined from density functional theory calculations as discussed in the Theoretical Calculations section. The average vibrational energy at 298 K of the $M^+(C_6H_5F)_x$ complexes is given in the Supporting Information in Table S1. We have estimated the sensitivity of our analysis to the deviations from the true frequencies by scaling the calculated frequencies to encompass the range of average scaling factors needed to bring calculated frequencies into agreement with experimentally determined frequencies found by Pople et al.[61] Thus, the originally calculated vibrational frequencies were increased and decreased by 10% for the Li^+, Na^+, and K^+ complexes and by 20% for the Rb^+, and Cs^+ complexes. The corresponding change in the average vibrational energy is taken to be an estimate of one standard deviation of the uncertainty in vibrational energy (Table S1).

We also consider the possibility that collisionally activated complex ions do not dissociate on the time scale of our experiment (about 10^{-4} s but energy-dependent) by including statistical theories for unimolecular dissociation, specifically Rice−Ramsperger−Kassel−Marcus (RRKM) theory, into eq 1 as described in detail elsewhere.[40,62] This requires sets of rovibrational frequencies appropriate for the energized molecules and the transition states (TSs) leading to dissociation. The former sets are given in the Supporting Information in Tables S1 and S2, whereas we assume that the TSs are loose and productlike because the interaction between the alkali metal ion and the fluorobenzene ligand(s) is largely electrostatic (ion−dipole, ion−induced dipole, and ion−quadrupole interactions). Thus, the most appropriate model for the TS is a loose association of the alkali metal ion and neutral fluorobenzene fragments. This TS is located at the centrifugal barrier for the interaction of $M^+(C_6H_5F)_{x-1}$ with C_6H_5F. In this case, the TS vibrations used are the frequencies corresponding to the products, which are also found in Table S1. The transitional frequencies, those that become rotations of the completely dissociated products, are treated as rotors, a treatment that corresponds to a phase space limit (PSL) and is described in detail elsewhere.[40] Briefly, two of the transitional mode rotors have rotational constants equal to those of the neutral C_6H_5F product with axes perpendicular to the reaction coordinate and correspond to its 2-D rotational constant, 0.071 cm^{-1}. In the $M^+(C_6H_5F)$ systems, which yield one atomic product, these are the only two translational modes. For $M^+(C_6H_5F)_2$ complexes, three additional transitional modes exist. Two of these rotors are the rotational constants of the $M^+(C_6H_5F)$ product, again those with axes perpendicular to the reaction coordinate. Of the two rotational constants of the products with axes lying along the reaction coordinate, one is a transitional mode and is assigned as the remaining rotational constant of the C_6H_5F product (0.189 cm^{-1}). The other becomes the 1-D external rotor of the TS. These are listed in Table S2. The 2-D external rotational constant of the TS is determined by assuming that the TS occurs at the centrifugal barrier for interaction of $M^+(C_6H_5F)$ with the neutral C_6H_5F molecule, treated variationally as outlined elsewhere.[40] The 2-D external rotations are treated adiabatically but with centrifugal effects included, consistent with the discussion of Waage and Rabinovitch.[63] In the present work, the adiabatic 2-D rotational energy is treated using a statistical distribution with explicit summation over the possible values of the rotational quantum number, as described in detail elsewhere.[40]

The model represented by eq 1 is expected to be appropriate for translationally driven reactions[64] and has been found to reproduce CID cross sections well.[55,59,62,65−68] The model is convoluted with the kinetic energy distributions of both the reactant ion and neutral Xe atom, and a nonlinear least-squares analysis of the data is performed to give optimized values for the parameters σ_0, E_0, and n. The error associated with the measurement of E_0 is estimated from the range of threshold values determined for different zero-pressure extrapolated data sets, variations associated with uncertainties in the vibrational frequencies (scaling as discussed above), and the error in the absolute energy scale, 0.05 eV (lab). For analyses that include the RRKM lifetime effect, the uncertainties in the reported E_0 values also include the effects of increasing and decreasing the time assumed available for dissociation by a factor of 2.

Equation 1 explicitly includes the internal energy of the ion, E_i. All energy available is treated statistically, which should be a reasonable assumption because the internal (rotational and vibrational) energy of the reactants is redistributed throughout the ion upon impact with the Xe atom. The threshold for dissociation is by definition the minimum energy required

leading to dissociation and thus corresponds to formation of products with no internal excitation. The threshold energies for dissociation reactions determined by analysis with eq 1 are converted to 0 K bond energies by assuming that E_0 represents the energy difference between reactants and products at 0 K.[69] This assumption requires that there are no activation barriers in excess of the endothermicity of dissociation, which should be valid for the simple noncovalent bond fission reactions examined here.[70]

Theoretical Calculations. To obtain model structures, vibrational frequencies, rotational constants, and energetics for the neutral C_6H_5F ligand and for the $M^+(C_6H_5F)_x$ complexes, ab initio and density functional theory calculations were performed using Gaussian 98.[71] Geometry optimizations were performed at the B3LYP/6-31G* level[72,73] for the $M^+(C_6H_5F)_x$ complexes where $M^+ = Li^+$, Na^+, and K^+. For complexes containing Rb^+ and Cs^+, geometry optimizations were performed with a hybrid basis set in which the effective core potentials (ECP) and valence basis sets of Hay and Wadt were used to describe the metal ion,[74] while 6-31G* basis sets were used for C, F and H atoms. As suggested by Glendening et al.,[75] a single polarization (d) function was added to the Hay−Wadt valence basis set for Rb and Cs, with exponents of 0.24 and 0.19, respectively.

Vibrational analyses of the geometry-optimized structures were performed to determine the vibrational frequencies for the neutral C_6H_5F ligand and the $M^+(C_6H_5F)_x$ complexes for $M^+ = Li^+$, Na^+, and K^+. The vibrational frequencies for the $M^+(C_6H_5F)_x$ complexes where $M^+ = Rb^+$ and Cs^+ were estimated by scaling the calculated frequencies for the analogous $K^+(C_6H_5F)_x$ complexes by a procedure described in detail previously.[76] When used to model data or calculate thermal energy corrections, the calculated vibrational frequencies were scaled by a factor of 0.9804.[77] The vibrational frequencies and rotational constants of neutral C_6H_5F and all $M^+(C_6H_5F)_x$ complexes are listed in the Supporting Information in Tables S1 and S2, respectively. Single-point energy calculations were performed at the MP2(full)/6-311+G(2d,2p) level with the B3LYP/6-31G* and B3LYP/Hybrid (6-31G*, Hay−Wadt) optimized geometries. To obtain accurate BDEs, zero-point energy (ZPE) corrections were applied and basis-set superposition errors (BSSE) were subtracted from the computed dissociation energies in the full counterpoise correction.[78,79] The ZPE corrections are small and decrease with increasing size of the alkali metal ion and are 6.2, 3.3, 2.2, 1.9, and 1.6 kJ/mol for the $M^+(C_6H_5F)$ complexes and 3.0, 2.7, 1.9, 1.9, and 2.0 kJ/mol for the $M^+(C_6H_5F)_2$ complexes, where $M^+ = Li^+$, Na^+, K^+, Rb^+, and Cs^+, respectively. The BSSE corrections are significantly larger, decrease with increasing size of the metal ion, and range from 4.3 to 21.6 kJ/mol. Calculations of the corresponding σ-binding complexes were also performed for the $M^+(C_6H_5F)$ complexes. In these complexes, the ZPE corrections are somewhat smaller than for the cation−π complexes, and are 2.4, 1.0, 0.5, 0.5, and 0.8 kJ/mol, respectively. The BSSE corrections are also smaller than for the cation−π complexes and range from 3.0 to 6.6 kJ/mol.

Results

Cross Sections for Collision-Induced Dissociation. Experimental cross sections were obtained for the interaction of Xe with 10 $M^+(C_6H_5F)_x$ complexes, where $M^+ = Li^+$, Na^+, K^+, Rb^+, and Cs^+, and $x = 1$ and 2. Figure 2 shows representative data for the $Na^+(C_6H_5F)_x$ complexes where $x = 1$ and 2. The other $M^+(C_6H_5F)_x$ complexes show relative behavior similar to that of $Na^+(C_6H_5F)_x$ and are included in the Supporting Information as Figure S1. The sequential loss of intact fluorobenzene molecules and ligand exchange with Xe are the only processes observed in these systems over the collision energy range studied, typically from 0 to >5 eV. The primary (most favorable) process observed for all of these complexes is the loss of a single intact fluorobenzene molecule in the CID reactions:

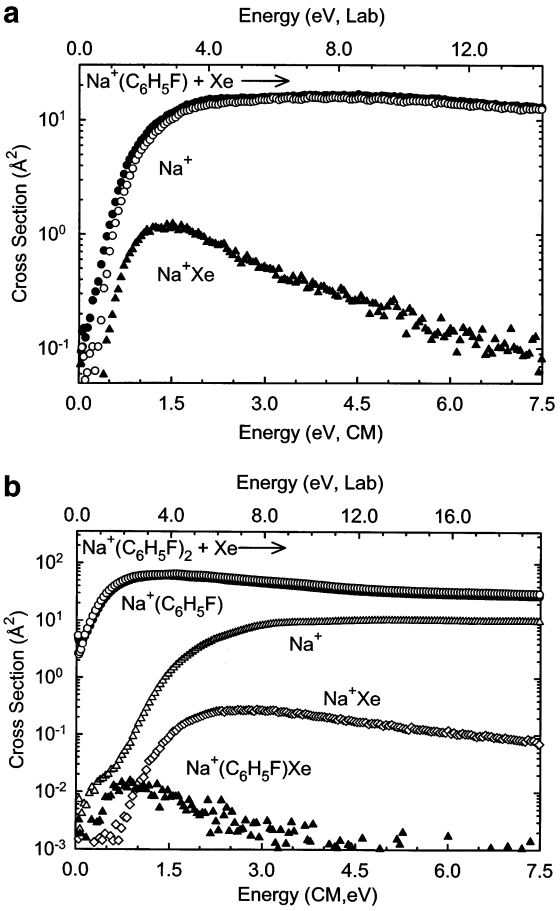

Figure 2. Cross sections for collision-induced dissociation of $Na^+(C_6H_5F)_x$, $x = 1$ and 2 (panels a and b, respectively), with Xe as a function of kinetic energy in the center-of-mass frame (lower *x*-axis) and the laboratory frame (upper *x*-axis). Data are shown for Xe pressures of ~0.2 and ~0.1 mTorr, for the $x = 1$ and 2 complexes, respectively. Primary and secondary product cross sections are shown as ● and △, respectively. Primary and secondary ligand exchange product cross sections are shown as ▲ and ◇, respectively. Data are also shown for the primary product cross section, extrapolated to zero pressure of Xe, as ○.

$$M^+(C_6H_5F)_x + Xe \rightarrow M^+(C_6H_5F)_{x-1} + C_6H_5F + Xe \quad (2)$$

The maximum cross section for reaction 2, as well as the total cross section, roughly doubles in magnitude from the mono to the bis complexes. The threshold for reaction 2 also decreases from the mono to bis complexes, consistent with conventional ideas of ligation of gas-phase ions, i.e., stepwise sequential bond energies decrease because of increasing electrostatic repulsion between the ligands, causing the distance between the cation and ligands to increase. Such ideas have been noted in previous experimental and theoretical studies of $M^+(ligand)_n$ clusters.[49,50,80−83]

$M^+(C_6H_5F)$ + Xe. Results for the interaction of $Na^+(C_6H_5F)$ with Xe are shown in Figure 2a. The major product is Na^+. The Na^+ product cross section has an apparent threshold of 0.12

TABLE 1: Fitting Parameters of Equation 1, Threshold Dissociation Energies at 0 K, and Entropies of Activation at 1000 K[a]

reactant complex	σ_0[b]	n[b]	E_0[c] (eV)	E_0(PSL) (eV)	kinetic shift (eV)	$\Delta S^{\ddagger}$(PSL) (J mol^{-1} K^{-1})
$Li^+(C_6H_5F)$	1.14 (0.2)	1.5 (0.1)	1.57 (0.22)	1.52 (0.21)	0.05	45 (2)
$Na^+(C_6H_5F)$	15.9 (0.5)	1.4 (0.1)	0.72 (0.03)	0.72 (0.03)	0.00	39 (2)
$K^+(C_6H_5F)$	32.5 (0.8)	1.1 (0.1)	0.57 (0.03)	0.57 (0.03)	0.00	32 (2)
$Rb^+(C_6H_5F)$	24.0 (0.7)	1.1 (0.1)	0.55 (0.03)	0.55 (0.03)	0.00	40 (2)
$Cs^+(C_6H_5F)$	12.9 (0.2)	1.6 (0.1)	0.52 (0.03)	0.52 (0.02)	0.00	44 (2)
$Li^+(C_6H_5F)_2$	72.2 (5.3)	1.2 (0.1)	1.03 (0.05)	0.99 (0.03)	0.04	39 (5)
$Na^+(C_6H_5F)_2$	92.8 (3.4)	1.1 (0.1)	0.69 (0.05)	0.68 (0.04)	0.01	24 (5)
$K^+(C_6H_5F)_2$	87.0 (1.7)	1.1 (0.1)	0.54 (0.04)	0.52 (0.03)	0.02	5 (5)
$Rb^+(C_6H_5F)_2$	23.7 (2.0)	1.2 (0.1)	0.51 (0.09)	0.49 (0.05)	0.02	5 (9)
$Cs^+(C_6H_5F)_2$	28.1 (0.8)	1.3 (0.1)	0.48 (0.01)	0.46 (0.04)	0.02	9 (9)

[a] Uncertainties are listed in parentheses. [b] Average values for loose PSL transition state. [c] No RRKM analysis.

eV and exhibits a maximum cross section of ~16 Å^2. The apparent thresholds for the analogous CID process in the other $M^+(C_6H_5F)$ complexes decrease regularly as the size of the cation increases, such that $Li^+(C_6H_5F)$ exhibits the largest apparent threshold of 1.1 eV, and $Cs^+(C_6H_5F)$ exhibits the smallest apparent threshold of <0.1 eV. In general, the cross section maxima for other $M^+(C_6H_5F)$ increase with the size of the cation, such that the cross section maximum is the smallest for $Li^+(C_6H_5F)$, ~2.5 Å^2, and the largest for $K^+(C_6H_5F)$, ~23 Å^2. The $Rb^+(C_6H_5F)$ and $Cs^+(C_6H_5F)$ complexes deviate from this simple trend, exhibiting maximum cross sections intermediate between those observed for the Na^+ and K^+ complexes, ~20 and 19 Å^2, respectively. The ligand exchange product Na^+Xe is observed with an apparent threshold of 0.6 eV and a maximum cross section of 1.1 Å^2 at 0.2 eV, which drops off rapidly with energy due to competition with the primary CID process. The apparent thresholds for the analogous ligand exchange process in the other $M^+(C_6H_5F)$ complexes decrease regularly as the size of the cation increases, such that Li^+Xe exhibits the largest apparent threshold of 1.5 eV, and both $Rb^+(C_6H_5F)$ and $Cs^+(C_6H_5F)$ exhibit the smallest apparent thresholds of <0.1 eV. The cross section maxima for other M^+Xe products are small and range from 1.0 to <0.1 Å^2 for the other $M^+(C_6H_5F)$ complexes.

$M^+(C_6H_5F)_2$ + Xe. Results for the interaction of $Na^+(C_6H_5F)_2$ with Xe are shown in Figure 2b. The primary product observed at all energies is $Na^+(C_6H_5F)$, corresponding to loss of an intact C_6H_5F molecule. The $Na^+(C_6H_5F)$ product has an apparent threshold near or below 0 eV, such that the cross section is nonzero at 0 eV. The apparent threshold for the analogous CID process in the other $M^+(C_6H_5F)_2$ complexes exhibits similar behavior in that the cross section magnitude is nonzero at 0 eV for all of the alkali metal ions except Li^+, which exhibits an apparent threshold of ~0.1 eV. In fact, the cross section magnitude at 0 eV and at all energies is found to increase with increasing size of the metal ion and is more than twice as large as that measured for the monoligated systems. However, the Rb^+ and Cs^+ systems again deviate from this trend, exhibiting a cross section that is smaller than those for the other metal ions. The maximum cross section observed varies from 38 to 66 Å^2 across these systems. The cross section for the primary product is observed to decline as the secondary CID product, Na^+, is formed, indicating that this product is formed sequentially from the primary CID product. The Na^+ product has an apparent threshold of 0.4 eV and reaches a maximum cross section of 10 Å^2 at the highest energies examined. The other $M^+(C_6H_5F)_2$ complexes show similar relative behavior such that the primary product declines as the secondary CID product, M^+, appears. The cross section maxima of the secondary CID products vary from 1.2 to 12 Å^2 across these systems.

In addition to the CID processes, ligand exchange reactions are also observed, producing the primary ligand exchange product, $Na^+(C_6H_5F)Xe$, as well as the secondary ligand exchange product, Na^+Xe (Figure 2b). The primary ligand exchange product, $Na^+(C_6H_5F)Xe$, has an apparent threshold near 0.2 eV, reaches a maximum cross section of ~0.02 Å^2, and then falls off rapidly due to competition with the primary CID process as well as sequential dissociation to produce the secondary ligand exchange product, Na^+Xe. The secondary ligand exchange product slowly grows in from an apparent threshold of ~0.7 eV and reaches a maximum cross section of 0.3 Å^2 at approximately 2.5 eV. At higher energies, it falls off due to competition with the secondary CID process. The other $M^+(C_6H_5F)_2$ complexes show similar relative behavior; however, the reactant ion beam intensities were much smaller for the $Rb^+(C_6H_5F)_2$ and $Cs^+(C_6H_5F)_2$ complexes, making it impossible to distinguish the primary ligand exchange products, $M^+(C_6H_5F)Xe$, from noise in these systems. The cross section magnitudes of the ligand exchange products are quite small. The primary and secondary ligand exchange products are approximately 3 and 2 orders of magnitude smaller than the primary CID product, respectively.

Threshold Analysis. The model of eq 1 was used to analyze the thresholds for reaction 2 in 10 $M^+(C_6H_5F)_x$ systems. As previously discussed,[59,62,65] the analysis of the primary CID thresholds provides the most reliable thermochemistry for such CID studies. This is because secondary and higher order products are more sensitive to lifetime effects, and additional assumptions are needed to quantitatively include the multiple products formed. The results of these analyses are given in Table 1 for all 10 $M^+(C_6H_5F)_x$ complexes. Representative fits to eq 1 for the $Na^+(C_6H_5F)_x$ complexes are shown in Figure 3. A comparable set of figures for the other $M^+(C_6H_5F)_x$ complexes is available in the Supporting Information as Figure S2. Experimental cross sections for the primary dissociation processes of the $M^+(C_6H_5F)_x$ complexes are accurately reproduced by a loose PSL TS model.[40] This model has been shown to provide the most accurate determination of kinetic shifts for CID reactions for electrostatically bound metal−ligand complexes.[36,40,67,68,84−87] The data are accurately reproduced over energy ranges exceeding 1 eV and over cross section magnitudes of a factor of at least 100 for all complexes except $Rb^+(C_6H_5F)_2$ and $Cs^+(C_6H_5F)_2$ because these cross sections are already nonzero at 0 eV. Threshold values, E_0, obtained from analyses of the data without consideration of lifetime effects are also included in Table 1. The difference between these values and those obtained when lifetime effects are included, E_0(PSL), the kinetic shift, is also given in Table 1. Although the $M^+(C_6H_5F)$ and $M^+(C_6H_5F)_2$ complexes have 33 and 69 vibrational modes, respectively, the kinetic shifts observed for these systems are

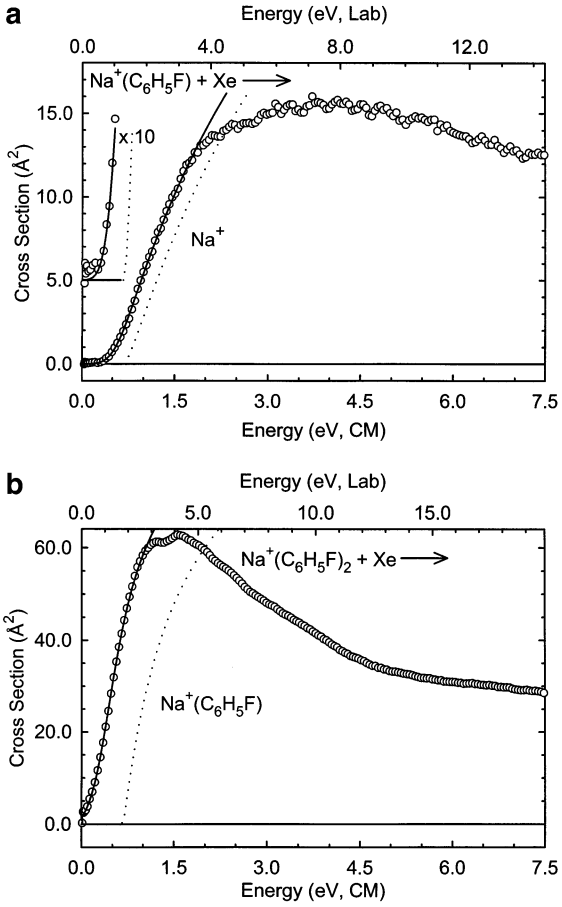

Figure 3. Zero-pressure extrapolated cross sections for the primary collision-induced dissociation product of the $Na^+(C_6H_5F)_x$ complexes, $x = 1$ and 2 (panels a and b, respectively), with Xe in the threshold region as a function of kinetic energy in the center-of mass frame (lower *x*-axis) and the laboratory frame (upper *x*-axis). Solid lines show the best fits to the data using the model of eq 1 convoluted over the neutral and ion kinetic and internal energy distributions. Dashed lines show the model cross sections in the absence of experimental kinetic energy broadening for reactants with an internal energy of 0 K.

quite small. In fact, of the monoligated complexes, only $Li^+(C_6H_5F)$, the most strongly bound complex, exhibits a kinetic shift (0.05 eV). All of the bis complexes exhibit small kinetic shifts that vary from 0.01 to 0.04 eV. The kinetic shifts decrease with increasing size of the cation, from Li^+ to Cs^+. This is easily understood because the observed kinetic shift should directly correlate with the density of states of the complex at threshold, which depends on the measured BDE, as shown in Table 1.

The entropy of activation, $\Delta S^{\ddagger}$, is a measure of the looseness of the TS. It is also a reflection of the complexity of the system because it is largely determined by the molecular parameters used to model the energized molecule and the TS but also depends on the threshold energy. The $\Delta S^{\ddagger}$(PSL) values at 1000 K are listed in Table 1 and vary between 5 and 45 J K^{-1} mol^{-1}. These entropies of activation compare favorably to an expanding range of noncovalently bound metal−ligand complexes previously measured in our laboratory and to those collected by Lifshitz[88] for simple bond cleavage reactions of ions.

Theoretical Results. Theoretical structures for neutral fluorobenzene and for the mono- and bisligated complexes of fluorobenzene with Li^+, Na^+, K^+, Rb^+, and Cs^+ were calculated as described above. Details of the geometry-optimized structures for each of these species are given in Table 2. The most stable structures for the $Na^+(C_6H_5F)$ and $Na^+(C_6H_5F)_2$ complexes are shown in Figure 4. The metal atom binds to the π cloud of the

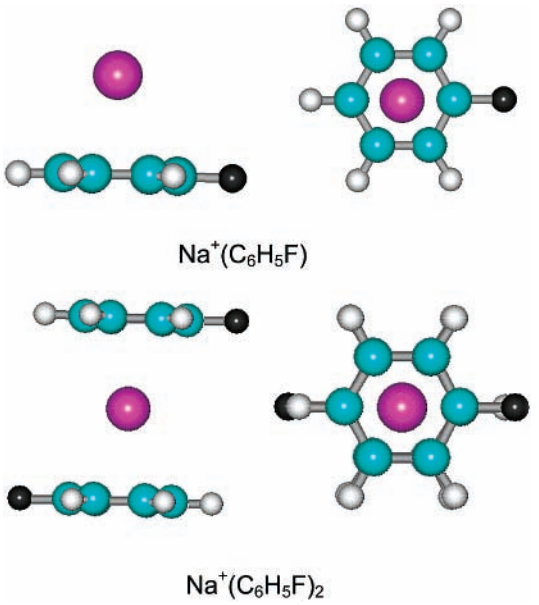

Figure 4. Ground-state B3LYP/6-31G* optimized geometries of $Na^+(C_6H_5F)_x$ complexes, where $x = 1$ and 2. Two views of each optimized structure are shown.

aromatic ring of the fluorobenzene molecule, a cation−π interaction. The distortion of the fluorobenzene molecule that occurs upon complexation to the alkali metal ion is minor. The change in geometry is largest for Li^+ and decreases with increasing size of the metal ion. The C−C bond lengths in the aromatic ring of fluorobenzene were found to increase by 0.004−0.010 Å upon complexation to the alkali metal ion as compared to the free ligand (Table 2). The alkali metal ion appears to have no influence on the aromatic C−H bond length (1.090 Å). As summarized in Table 2, M^+−C and M^+−ring centroid distances[89] and C−F bond lengths are found to increase as the size of the metal ion increases for both the mono and bis complexes. These distances are also found to increase on going from the mono to the corresponding bis complexes. In contrast to that found for the analogous benzene systems,[20] out-of-plane bending of the ring hydrogen atoms is found to decrease with increasing size of the metal ion for both the mono and bis complexes. Furthermore, out-of-plane bending of the ring hydrogen atoms is smaller than for the analogous benzene complexes and is smaller for the bis complexes than the for the mono complexes. This makes sense because the alkali metal ion is further away from the ring in the complexes to fluorobenzene than it is in the complexes to benzene. The same is true for the bisligated complexes as compared to the monoligated complexes. The longer M^+−ring centroid distance results in the metal ion exerting a smaller influence on the ligand.

As can be seen in Figure 4, the ground-state structure of $Na^+(C_6H_5F)$ has the Na^+ ion interacting with the π cloud of the aromatic ring. However, it is possible that the metal ion might interact with a lone pair of electrons on the fluorine atom through a σ-type interaction. Stable σ-binding conformers were calculated for the Li^+, Na^+, K^+, Rb^+, and Cs^+ complexes to fluorobenzene at the B3LYP/6-31G* level. The optimized structure of the σ-binding conformer of $Na^+(C_6H_5F)$ is shown in Figure 5. In these σ-binding complexes, the metal ion lies in the plane of ring and is oriented along the dipole moment of the fluorobenzene ligand. At the MP2(full)/6-311+G(2d,2p) level of theory, the σ-binding conformers are found to be 16.9, 4.4, and 3.5 kJ/mol less stable than the corresponding cation−π complexes for Li^+, Na^+, and K^+, respectively. In contrast, the

TABLE 2: Geometrical Parameters of B3LYP/6-31G* Optimized Structures of the $M^+(C_6H_5F)_x$ Complexes

complex	M^+−C (Å)	M^+−centroid[a] (Å)	M^+−F (Å)	C−H (Å)	CH OOP[b] (deg)	C−F (Å)	C−C (Å)
C_6H_5F				1.090	0.000	1.351	1.394
$Li^+(C_6H_5F)$	2.384	1.932		1.090	0.601	1.329	1.404
$Li^+(C_6H_5F)$[c]			1.729	1.090	0.089	1.440	1.391
$Na^+(C_6H_5F)$	2.791	2.414		1.090	0.365	1.335	1.402
$Na^+(C_6H_5F)$[c]			2.088	1.090	0.080	1.415	1.392
$K^+(C_6H_5F)$	3.229	2.911		1.090	0.280	1.341	1.400
$K^+(C_6H_5F)$[c]			2.483	1.090	0.073	1.398	1.393
$Rb^+(C_6H_5F)$[d]	3.515	3.225		1.090	0.257	1.343	1.399
$Rb^+(C_6H_5F)$[c,d]			2.749	1.090	0.132	1.389	1.393
$Cs^+(C_6H_5F)$[d]	3.788	3.517		1.090	0.214	1.345	1.398
$Cs^+(C_6H_5F)$[c,d]			2.982	1.090	0.137	1.384	1.394
$Li^+(C_6H_5F)_2$	2.498	2.067		1.090	0.368	1.335	1.402
$Na^+(C_6H_5F)_2$	2.842	2.472		1.090	0.342	1.338	1.401
$K^+(C_6H_5F)_2$	3.263	2.949		1.090	0.251	1.342	1.399
$Rb^+(C_6H_5F)_2$[d]	3.541	3.255		1.090	0.233	1.344	1.399
$Cs^+(C_6H_5F)_2$[d]	3.812	3.546		1.090	0.192	1.346	1.399

[a] The metal ring−centroid distance is defined as the distance from the metal atom to the central point within the aromatic ring of toluene that is in the plane of the carbon atoms. [b] Out-of-plane angle. [c] Complexes in which the alkali metal cation binds to the fluorine atom via a σ-type interaction. [d] The Hay−Wadt ECP/valence basis set was used for the metal ion, as described in the text, and the 6-31G* basis set for C and H.

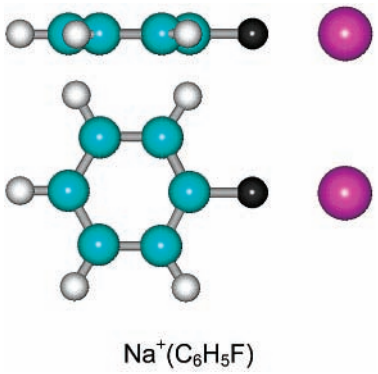

Figure 5. B3LYP/6-31G* optimized geometry of the σ-type binding conformer of the $Na^+(C_6H_5F)$ complex. Two views of the optimized structure are shown.

σ-binding conformers for Rb^+ and Cs^+ are found to be 3.2 and 0.8 kJ/mol more stable than the corresponding cation−π complexes, respectively. If ZPE and BSSE corrections are not included, the cation−π complexes of Rb^+ and Cs^+ are 0.9 and 1.5 kJ/mol more stable than the σ-binding conformers, respectively. Thus the relative stability of these σ-binding and cation−π conformers varies with the size of the cation.

As can also be seen in Figure 4, the lowest energy structure for the $Na^+(C_6H_5F)_2$ complex has the fluorine atoms oriented anti to one another to minimize repulsive ligand−ligand interactions associated with the fluorine atoms. The anti configuration was found to be the lowest energy structure for all of the bis complexes. To estimate the barrier to free rotation of the aromatic ring in the bisligated complexes, optimizations were performed for $Li^+(C_6H_5F)_2$ with the fluorine atoms oriented syn, "ortho", and "meta" to one another. The complexes with the fluorine atoms oriented syn, "ortho", and "meta" to one another were found to be 0.8, 1.0, and 1.0 kJ/mol less stable than the ground-state anti complex, respectively. Therefore, at room temperature these complexes should have sufficient energy to freely interconvert (see Table S1).

Theoretical estimates for the $M^+(C_6H_5F)_x$ BDEs were determined using the B3LYP/6-31G* geometries and single-point energy calculations at MP2(full)/6-311+G(2d,2p). In earlier work in which we measured and calculated the strength of cation−π interactions in M^+(toluene)$_x$ complexes, we found better correlation between the theoretical and experimental results for energetics based on MP2(full)/6-311+G(2d,2p) theory than for B3LYP/6-311+G(2d,2p) results.[24] These results are listed in Table 3, along with the experimental determinations performed here for fluorobenzene and other theoretical results found in the literature.[31] Results shown in Table 3 also include ZPE and BSSE corrections. The mean absolute deviation (MAD) between the experimental and theoretical values for all 10 complexes is 6.8 ± 7.4 kJ/mol. This is slightly larger than the average experimental error of 5.5 ± 5.2 kJ/mol. The MAD is larger for the mono complexes, 10.0 ± 9.0 kJ/mol, than for the bis complexes, 3.7 ± 4.3 kJ/mol. Inspection of the data makes it clear than the Li^+ complex is the principal contributor to the large deviations for the mono complexes. Excluding the Li^+ complex, the mono complexes exhibit a MAD of 6.2 ± 3.2 kJ/mol. The poorer agreement for the $Li^+(C_6H_5F)$ complex most likely results from the difficulty associated with efficient detection of this low-mass ion as described earlier.[22] Previous calculations for the $Na^+(C_6H_5F)$ complex performed at MP2/6-31G**//HF/6-31G** and HF/6-31G**//HF/6-31G** levels of theory by Dougherty and co-workers[31] differ from the value calculated here and are in poorer agreement with our measured value. Both of their values are higher than that calculated here, by 18.5 and 5.1 kJ/mol, respectively. The higher level of theory employed here provides a BDE for $Na^+(C_6H_5F)$ that is in much better agreement with the experimental value and is only 4.1 kJ/mol higher than the measured value.

Discussion

Trends in Experimental $M^+(C_6H_5F)_x$ Bond Dissociation Energies. The 0 K experimental BDEs of the $M^+(C_6H_5F)_x$ complexes are summarized in Table 3. The variation in the measured BDEs with the size of the alkali metal ion is shown in Figure 6 for both the mono and bis complexes. The M^+−(C_6H_5F) and $(C_6H_5F)M^+$−(C_6H_5F) BDEs are found to decrease monotonically as the size of the metal ion increases from Li^+ to Cs^+. This is the expected trend for binding based primarily on electrostatic interactions. The increasing size of the alkali metal ion[90] leads to larger metal−ligand bond distances (see Table 2), and the nonlinear distance dependencies of the electrostatic interactions fall off rapidly, as R^{-2} for ion−dipole, R^{-3} for the ion−quadrupole, and R^{-4} for ion−induced dipole interactions, resulting in weaker binding interactions in the cation−π complexes for the larger alkali metal ions.

The BDEs of the bis complexes are smaller than the corresponding mono complexes in all cases. The decrease in

TABLE 3: Bond Dissociation Enthalpies of $M^+(C_6H_5F)_x$ (x = 1 and 2) at 0 K

	experiment (TCID), kJ/mol		theory, X = F, kJ/mol			
complex	X = F[a]	X = H[b]	D_e[c]	D_0[c,d]	$D_{0,BSSE}$[c,e]	D_e
$Li^+(C_6H_5X)$	146.9 (20.1)	161.1 (13.5)	138.6	132.4	121.7	
			113.2[f]	110.8[f]	104.8[f]	
$Na^+(C_6H_5X)$	69.7 (3.3)	92.6 (5.8)	86.9	83.6	73.8	105.4[i]
		88.3 (4.3)[g]				92.0[j]
			77.0[f]	76.0[f]	69.4[f]	
$K^+(C_6H_5X)$	55.1 (3.0)	73.3 (3.8)	65.4	63.2	57.8	
			58.5[f]	58.0[f]	54.3[f]	
$Rb^+(C_6H_5X)$[h]	53.6 (5.2)	68.5 (3.8)	52.7	50.8	45.0	
			51.8[f]	51.3[f]	48.2[f]	
$Cs^+(C_6H_5X)$[h]	50.2 (5.0)	64.6 (4.8)	46.8	45.2	40.9	
			45.3[f]	44.7[f]	41.7[f]	
$Li^+(C_6H_5X)_2$	95.1 (2.7)	104.2 (6.8)	120.1	117.1	95.5	
$Na^+(C_6H_5X)_2$	65.9 (3.8)	80.0 (5.8)	84.3	81.6	65.6	
$K^+(C_6H_5X)_2$	50.4 (3.0)	67.5 (6.8)	63.5	61.6	51.7	
$Rb^+(C_6H_5X)_2$[h]	47.1 (4.8)	62.7 (7.7)	51.1	49.2	40.0	
$Cs^+(C_6H_5X)_2$[h]	44.6 (4.3)	58.8 (7.7)	45.0	43.0	35.2	

[a] Present results, threshold collision-induced dissociation. Uncertainties are listed in parentheses. [b] Taken from Amicangelo and Armentrout, except as noted.[20] [c] Calculated at the MP2(full)/6-311+G(2d, 2p) level of theory using B3LYP/6-31G* optimized geometries. [d] Including zero-point energy corrections with B3LYP/6-31G* frequencies scaled by 0.9804. [e] Also includes basis set superposition error corrections. [f] σ-binding conformer. [g] Armentrout and Rodgers.[19] [h] The Hay−Wadt ECP/valence basis set was used for the metal ion, as described in the text, and the 6-31G* basis set and 6-311+G(2d, 2p) basis set were used for C and H in geometry optimization and single-point energy calculations, respectively. [i] Mecozzi et al. calculated at the MP2/6-31G**//6-31G**. [j] HF/6-31G**//6-31G** levels of theory.[31]

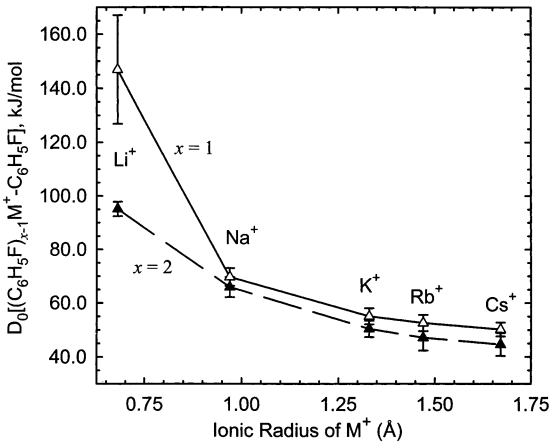

Figure 6. Bond dissociation energies at 0 K (in kJ/mol) of the $M^+(C_6H_5F)_x$ complexes plotted versus the ionic radius of M^+. Data are shown for x = 1 and 2 as △ and ▲, respectively. All values are taken from Table 3.

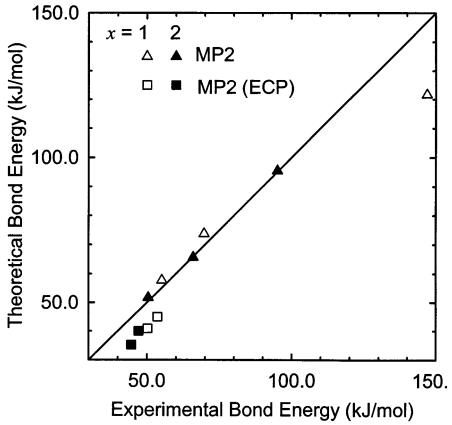

Figure 7. Theoretical versus experimental bond dissociation energies at 0 K (in kJ/mol) of the $M^+(C_6H_5F)_x$ complexes. The diagonal line indicates the values for which the calculated and measured bond dissociation energies are equal. All values are taken from Table 3.

the measured BDE on going from the mono- to the bisligated system is largest for the Li^+ complex and is fairly small and similar for the other alkali metal ions. The sequential BDEs are found to decrease by 51.8, 3.8, 4.7, 6.5, and 5.6 kJ/mol for the Li^+, Na^+, K^+, Rb^+, and Cs^+ systems, respectively. This trend is believed to be the result of Coulombic and dipole−dipole repulsions between ligands.[84] The distance between the aromatic rings is found to increase with increasing size of the metal ion, from ~4.13 Å in $Li^+(C_6H_5F)_2$ to 7.09 Å in $Cs^+(C_6H_5F)_2$ (Table 2, twice the M^+−centroid distance). Clearly, the magnitude of the repulsive ligand−ligand interactions for $Li^+(C_6H_5F)_2$ should be larger than those of the other $M^+(C_6H_5F)_2$ complexes and should also decrease with increasing size of the alkali metal ion. This should result in smaller differences in the BDEs for the mono- and bisligated complexes as the size of the alkali metal ion increases. The very small difference observed for Na^+, K^+, Rb^+, and Cs^+ suggests that the ligand−ligand repulsions are very similar and minor for these complexes.

Comparison of Theory and Experiment. The experimentally determined and theoretically calculated $M^+(C_6H_5F)_x$ BDEs are listed in Table 3. The agreement between the experimental BDEs and theoretical values determined at MP2(full)/6-311+G(2d,2p)//B3LYP/6-31G* level is illustrated in Figure 7. The theoretical calculations are in qualitative agreement with the observed trends in experimental BDEs discussed in the previous section. Quantitatively, the agreement between the experimental BDEs and the six theoretical $M^+(C_6H_5F)_x$ BDEs calculated including all electrons (M^+ = Li^+, Na^+, and K^+; x = 1 and 2) is very good, with a mean absolute deviation (MAD) of 5.7 ± 9.7 kJ/mol. These differences are slightly smaller than the average experimental error in these values of 6.0 ± 6.9 kJ/mol. The low theoretical BDE for $Li^+(C_6H_5F)$ as compared to the experimental value (a difference of 25.2 kJ/mol) is disappointing. If this value is not included, the MAD drops to 1.8 ± 1.7 kJ/mol, well within the average experimental error of 3.2 ± 0.4 kJ/mol. This poorer agreement may arise for two reasons. One is the experimental difficulty in measuring cross sections for Li^+ as a result of the difficulty associated with efficient detection of this light mass.[22] An alternative explanation is that theory may systematically underestimate the bond energies for monoligated Li^+ complexes, as a result of the higher degree of covalency in the metal−ligand bond. This is shown by the

TABLE 4: Enthalpies and Free Energies of Binding of $M^+(C_6H_5F)_x$ ($x = 1$ and 2) at 0 and 298 K[a]

reactant complex	ΔH_0[b]	$\Delta H_{298} - \Delta H_0$[c]	ΔH_{298}	$T\Delta S_{298}$[c]	ΔG_{298}
$Li^+(C_6H_5F)$	146.9 (20.1)	2.7 (2.9)	149.6 (20.3)	32.9 (6.6)	116.7 (21.4)
$Na^+(C_6H_5F)$	69.7 (3.3)	1.0 (2.3)	70.7 (4.1)	28.0 (6.7)	42.7 (7.9)
$K^+(C_6H_5F)$	55.1 (3.0)	0.4 (2.0)	55.5 (3.6)	26.0 (6.9)	29.4 (7.8)
$Rb^+(C_6H_5F)$	53.6 (5.2)	0.4 (1.8)	53.9 (5.5)	27.7 (7.0)	26.2 (8.9)
$Cs^+(C_6H_5F)$	50.2 (5.0)	0.4 (1.8)	50.5 (5.3)	28.4 (6.5)	22.1 (8.4)
$Li^+(C_6H_5F)_2$	95.1 (2.7)	−3.0 (2.2)	92.1 (3.5)	34.8 (12.2)	57.2 (12.7)
$Na^+(C_6H_5F)_2$	65.9 (3.8)	−3.1 (2.1)	62.8 (4.3)	30.9 (12.3)	31.9 (13.0)
$K^+(C_6H_5F)_2$	50.4 (3.0)	−3.4 (1.6)	47.0 (3.5)	25.8 (11.2)	21.2 (11.7)
$Rb^+(C_6H_5F)_2$	47.1 (4.8)	−3.5 (1.1)	43.6 (4.9)	25.4 (13.8)	18.2 (14.6)
$Cs^+(C_6H_5F)_2$	44.6 (4.3)	−3.7 (1.1)	40.9 (4.4)	26.4 (13.8)	14.5 (14.5)

[a] Values are given in kJ/mol. Uncertainties are listed in parentheses. [b] Present experimental results (Table 3). [c] Density functional values from calculations at the B3LYP/6-31G* level of theory with frequencies scaled by 0.9804. The Hay−Wadt ECP/valence basis set was used for Rb^+ and Cs^+.

calculated partial charge on M^+, which is 0.80e for $Li^+(C_6H_5F)$ and varies between 0.90e and 0.99e for all other $M^+(C_6H_5F)_x$ complexes. Therefore, higher levels of theory may be required to accurately describe the binding in this complex, a conclusion also drawn for Li^+ complexes with a variety of other ligands.[22,24,43,45,47]

The agreement between the experimental BDEs and the theoretical values calculated from the Hay−Wadt ECP/valence basis set for the metal ions (Rb^+ and Cs^+) is not as good. A MAD of 8.6 ± 1.1 kJ/mol is found. This is nearly twice as large as the average experimental error in these values of 4.8 ± 0.4 kJ/mol. It is clear from Table 3 and Figure 7 that the Hay−Wadt ECP/valence basis set results in calculated BDEs that are too low. The deviations between the theoretical and experimental values are slightly larger for Cs^+ than for Rb^+. These observations suggest that the Hay−Wadt ECP/valence basis set introduces systematic errors in the determination of alkali metal binding affinities to fluorobenzene. Similar results were found for the analogous benzene[20] and toluene systems.[24]

Conversion from 0 to 298 K. To allow comparison to commonly used experimental conditions, we convert the 0 K bond energies determined here to 298 K bond enthalpies and free energies. The enthalpy and entropy conversions are calculated using standard formulas (assuming harmonic oscillator and rigid rotor models) and the vibrational and rotational constants determined for the B3LYP/6-31G* optimized geometries, which are given in the Supporting Information in Tables S1 and S2. Table 4 lists 0 and 298 K enthalpies, free energies, and enthalpic and entropic corrections for all systems experimentally determined (from Table 1). The uncertainties in the enthalpic and entropic corrections are determined by 10% variation in the molecular constants for complexes with Li^+, Na^+, and K^+ and by 20% variation in the molecular constants for complexes with Rb^+ and Cs^+. Because the metal−ligand frequencies are very low and may not be adequately described by theory, the listed uncertainties also include contributions from scaling these frequencies up and down by a factor of 2. The latter provides a conservative estimate of the computational errors in these low-frequency modes and is the dominant source of error in the uncertainties listed.

Influence of the Fluoro Substituent. The effect of the fluoro substituent on the cation−π interaction can be examined by comparing the results obtained here for fluorobenzene, C_6H_5F, to those obtained in earlier studies for benzene, C_6H_6,[20] and toluene, $C_6H_5CH_3$[24] (Figure 8). Benzene is a highly symmetric molecule and has no dipole moment. Substitution breaks up the symmetry in the molecule and results in a dipole moment for both toluene and fluorobenzene. The methyl substituent has only a minor effect and results in measured and calculated dipole moments of 0.36 ± 0.05 and 0.41 D, respectively.[24,52] In contrast, fluoro substitution perturbs the molecule to a much greater extent and results in a relatively large dipole moment for fluorobenzene. The measured value for the dipole moment of fluorobenzene is 1.60 ± 0.08 D,[52] significantly lower than the value calculated here, 1.91 D. However, the dipole moments of toluene and fluorobenzene lie in the plane of the aromatic ring, perpendicular to the binding interaction in the cation−π complexes. Therefore, an effective ion−dipole interaction of the alkali metal cation with these π ligands is not possible.

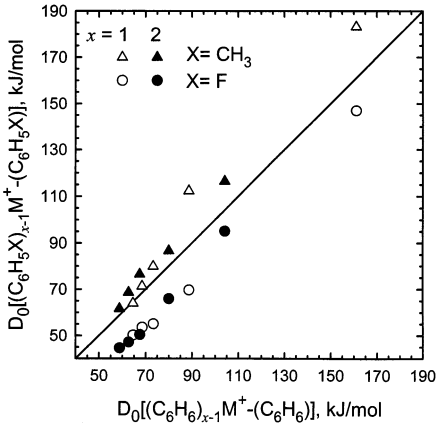

Figure 8. Bond dissociation energies (in kJ/mol) at 0 K of the $(C_6H_5X)_{x-1}M^+-(C_6H_5X)$ versus $(C_6H_6)_{x-1}M^+-(C_6H_6)$, where $X = CH_3$ as (△, ▲) and F as (○, ●), and $M^+ = Li^+$, Na^+, K^+, Rb^+, and K^+. Data are shown for $x = 1$ and 2, respectively. Values for C_6H_6 are taken from Amicangelo and Armentrout.[20] Values for $C_6H_5CH_3$ are taken from Amunugama and Rodgers.[24]

The polarizability of benzene is estimated using the additivity method of Miller[53] to be 9.99 Å^3 and increases to 12.26 Å^3 for toluene and slightly decreases to 9.86 Å^3 for fluorobenzene. Therefore, the ion-induced dipole interaction should result in stronger binding to toluene and weaker binding in fluorobenzene compared to that to benzene. If the ion-induced dipole interaction plays an important role in determining the strength of the cation−π interaction, then the BDEs should follow the order fluorobenzene < benzene < toluene in agreement with the measured and calculated BDEs for these ligands.

Dougherty and co-workers[1,2,31] have argued that the cation−π interactions are dominated by the interaction of the cation with the permanent quadrupole moment of the aromatic ligand. The quadrupole moment is a measure of the distribution of charge within the molecule relative to a particular axis. In the case of aromatic ligands, the relevant axis is the axis that passes through the center of the aromatic ring and is perpendicular to the plane of the aromatic ring. The experimental technique established for measuring the quadrupole moment of a molecule requires that the molecule have no dipole moment. Therefore, the

quadrupole moment has been measured for benzene (−8.60 DÅ) but cannot be measured for toluene or fluorobenzene. However, we can estimate the influence of the substituent on the permanent quadrupole moment of the aromatic ring by considering the inductive effects of the substituent. The methyl substituent of toluene acts as an electron donor and therefore leads to an increase in the π electron density of the aromatic ring and the quadrupole moment. In contrast, the fluoro substituent of fluorobenzene acts as an electron-withdrawing agent and therefore leads to a decrease in the π electron density of the aromatic ring and the quadrupole moment. Thus, the quadrupole moments of these aromatic ligands should follow the order fluorobenzene < benzene < toluene. Therefore, if the ion−quadrupole interaction dominates the cation−π interaction, then the strength of the cation−π interaction and the BDEs should follow this same order, in agreement with the measured and calculated BDEs for these ligands.

As discussed above, a cation−π interaction between an alkali metal ion and an aromatic ligand is expected to be largely electrostatic, arising from ion−dipole, ion−induced dipole, and ion−quadrupole interactions, but dominated by the ion−quadrupole interaction. The ion−dipole interaction is ineffective for the cation−π complexes examined here and should have very little influence upon the strength of the binding in these systems. However, the ion−induced dipole and ion−quadrupole interactions act in concert to increase the strength of the cation−π interaction in the toluene complexes and decrease the strength of these interactions in the fluorobenzene complexes as compared to the benzene complexes. The measured BDEs of the $M^+(C_6H_5X)_x$ complexes correlate directly with the influence of the substituent on the electron density of the aromatic π system and the polarizability of the aromatic ligand. From these results it is difficult to ascertain whether the quadrupole moment or the polarizability of the aromatic ligand is more influential in determining the strength of the cation−π interaction, but it is likely that both of these interactions play some role. The BDEs to toluene show a slight increase, and those to fluorobenzene show a modest decrease, compared to the analogous benzene complexes. The measured BDEs to $M^+(C_6H_5F)_x$ are smaller than the analogous $M^+(C_6H_6)_x$ BDEs in all cases. The decrement in the binding energy varies between 9.1 and 22.9 kJ/mol but is actually very similar for most complexes, 15.5 ± 3.4 kJ/mol. This contrasts with the behavior observed for the toluene complexes, where the increase in binding was largest for Li^+ and decreased with increasing size of the cation.[24]

***σ*-Binding versus Cation−*π* Complexes.** As discussed in the Theoretical Results section, σ-binding conformers are also found for these systems. The relative stabilities of the σ-binding versus cation−π complexes is such that at 298 K, the temperature of the reactant ions, the distribution of ions created in our source is probably a mixture of the σ-binding and cation−π complexes for all metal ions except Li^+. The relative populations of the σ-binding complexes for the Na^+ and K^+ systems is probably quite small, on the order of 5−10%. The small population of the σ-binding complexes present in our beam would tend to lower the measured threshold for the CID of these complexes. This effect should be fairly small as a result of the small differences in binding affinities and small population of σ-binding complexes. In contrast, the σ-binding and cation−π complexes are nearly degenerate for the Rb^+ and Cs^+ complexes, such that our ion beams may contain nearly equal populations of each of these conformers. Because the binding energies in the σ-binding and cation−π complexes to Rb^+ and Cs^+ are nearly equal, the effect on the threshold determination should be almost negligible. The presence of a significant population of σ-binding complexes to Rb^+ and Cs^+ is likely the reason for the smaller cross sections measured in these systems as compared to the smaller alkali metal cations. The σ-binding complexes are nearly 2-D structures and would be expected to have a smaller cross section than the analogous cation−π complexes. Thus, it seems likely that Rb^+ and Cs^+ would take on whichever conformation the local environment allowed, whereas the smaller alkali metal ions, Li^+, Na^+, and K^+, would preferentially bind via a cation−π interaction.

Comparison to Other Fluorinated Aromatic Ligands. As mentioned in the Introduction, studies of cation−π interactions of fluoro-substituted benzenes and toluenes have been fairly limited. In fact, previous studies of the alkali metal ions have been limited to theoretical calculations for Na^+ binding to fluorobenzene, 1,4-difluorobenzene, and 1,3,5-trifluorobenzene.[31] As these calculations were performed at lower levels of theory than employed here, the calculated values are not as reliable, but the relative BDEs should be fairly accurate. Mecozzi et al.[31] find that the binding to these fluoro-substituted benzenes is weaker than to benzene. In fact, the cation−π interaction becomes increasingly weaker as more fluoro substituents are added to the ring, such that the BDEs follow the order benzene > fluorobenzene > 1,4-difluorobenzene > 1,3,5-trifluorobenzene. These results are not surprising because each of the fluoro substituents will tend to remove electron density from the π cloud and therefore result in weaker cation−π binding. The relative binding energies calculated for the σ- and π-binding conformers of the alkali metal ions to fluorobenzene performed here suggest that the weakening of the cation−π interaction that occurs for the more highly substituted fluorobenzenes may make the σ-binding complexes more stable than the cation−π complexes. Other studies of cation−π interactions to fluoro-substituted benzenes and toluenes have been limited to Cr^+, Fe^+, Co^+, and Au^+.[31−35] In addition, the binding of Au^- to C_6F_6 has also been examined.[35] The binding in these complexes should be somewhat different than to the alkali metal ions because these ions possess valence electrons that participate in the binding interaction, resulting in much stronger BDEs. In the studies by Schwarz and co-workers,[33,34] fluorobenzene is found to bind to all three metal ions, Cr^+, Fe^+, and Co^+, less strongly than to benzene by 18.4, 18.8, and 20.5 kJ/mol, respectively. A similar decrease in the binding energies is observed upon fluoro substitution of toluene, where the decrease in binding affinity varies between 15.9 and 20.1 kJ/mol depending upon the site of substitution and the transition metal cation. In all cases, the BDEs to a given ligand follow the order $Cr^+ < Fe^+ < Co^+$. Similar trends have been observed for other σ- and π-binding ligands.[44,46,48,68] In the study by Dunbar and co-workers[32] on Cr^+ binding to substituted fluorobenzenes, they examined all possible fluoro-substituted variants. The trends in the strength of the cation−π interaction were similar to that summarized above for the Na^+ complexes. The strength of the cation−π interaction decreases as the extent of fluoro substitution increases. Small variations in the binding strength occur for the various isomers of difluoro-, trifluoro-, and tetrafluorobenzene. More significant is that when two or more fluorine atoms are located at adjacent sites on the ring, σ-binding to the fluorine atoms becomes more favorable than the cation−π interaction. In addition, the greater stability of the σ-binding conformer compared to the cation−π conformer increases with higher levels of fluoro substitution. Again, these observations are not surprising as each fluoro substituent withdraws electron

density from the π cloud and weakens the cation$-\pi$ interaction. The study by Ho and Dunbar[35] on Au^+ and Au^- binding to substituted fluorobenzenes was much more limited in scope. In this work, they examined only three complexes, $Au^+(C_6H_6)$, $Au^+(C_6F_5H)$, and $Au^-(C_6F_6)$. The binding of Au^+ was found to be quite strong compared to both the alkali and first-row transition metal ions. The binding is also much stronger to benzene than pentafluorobenzene, by 163 kJ/mol. Although not particularly relevant to the study of cation$-\pi$ binding to aromatic species, the measurement of binding energy of the $Au^-(C_6F_6)$ complex represents the first determination of anion$-\pi$ binding. In this case, the binding is weaker than cation$-\pi$ binding but may suggest that electronegative groups may also participate in the stabilization of protein structures. Thus, this observation suggests that additional stabilization of the protein structure might be gained when the side chains of arginine, lysine, asparagine, glutamine, and histidine interact with the aromatic residues of phenylalanine, tyrosine, and tryptophan even when the side chains of the former are not protonated.

Conclusions

The kinetic energy dependence of the collision-induced dissociation of $M^+(C_6H_5F)_x$ complexes ($M^+ = Li^+$, Na^+, K^+, Rb^+, and Cs^+; $x = 1$ and 2), with Xe is examined in a guided ion beam tandem mass spectrometer. The dominant dissociation pathway observed for all complexes is loss of an intact fluorobenzene molecule. Thresholds for these dissociation reactions are determined after careful consideration of the effects of reactant internal energy, multiple collisions with Xe, and the lifetime of the ionic reactants (using a loose PSL TS model). The molecular parameters needed for the analysis of experimental data, as well as structures and theoretical estimates of the BDEs for the $M^+(C_6H_5F)_x$ complexes, are obtained from theoretical calculations performed at the MP2(full)/6-311+G(2d,2p)//B3LYP/6-31G(d) level. The absolute $M^+-(C_6H_5F)$ and $(C_6H_5F)M^+-(C_6H_5F)$ bond dissociation energies are observed to decrease monotonically as the size of the alkali metal ion increases from Li^+ to Cs^+. Similarly, the difference in the BDEs of the mono and bis complexes is also observed to decrease monotonically with the size of the alkali metal ion. These trends are explained in terms of the electrostatic nature of the bonding in the $M^+(C_6H_5F)_x$ complexes and the changes in magnitude of the ligand$-$ligand interactions in the $M^+(C_6H_5F)_2$ complexes, respectively. Theoretical values of the $M^+(C_6H_5F)_x$ bond energies are also determined by ab initio calculations performed at the MP2(full)/6-311+G(2d,2p)//B3LYP/6-31G(d) level of theory for $M^+ = Li^+$, Na^+, and K^+. The agreement between experiment and theory is very good when full electron correlation is included for Li^+, Na^+, and K^+. However, significant deviations are observed for the $Li^+(C_6H_5F)$ complex. When effective core potentials are used, for Rb^+ and Cs^+, theory is found to underestimate the strength of the binding. Another interesting observation is that the σ-binding and cation$-\pi$ complexes of Rb^+ and Cs^+ to fluorobenzene are nearly degenerate, and therefore a mixture of these two conformers is probably accessed in our experiments. Comparisons made to experimental BDEs of the analogous benzene and toluene complexes reveal that the fluoro substituent leads to a decrease in the strength of the cation$-\pi$ interaction, in both the mono and bis complexes, to all of the alkali metal ions. Comparison to other studies suggests that the cation$-\pi$ interaction becomes progressively weaker with higher degrees of fluoro substitution of the aromatic ring. Indeed, σ-binding conformers become favored over cation$-\pi$ conformers whenever there are two or more adjacent fluorine atoms substituted on the ring.

Acknowledgment. This work was supported by the National Science Foundation, Grant 0138504.

Supporting Information Available: Tables of vibrational frequencies, average vibrational energies and rotational constants, and B3LYP/6-31G* geometry-optimized structures for neutral C_6H_5F and the $M^+(C_6H_5F)_x$ complexes, and figures showing cross sections for the collision-induced dissociation of $M^+(C_6H_5F)_x$ complexes with Xe as well as empirical fits to the primary product channels (where $M^+ = Li^+$, K^+, Rb^+, and Cs^+) (PDF). This material is available free of charge via the Internet at http://pubs.acs.org.

References and Notes

(1) Ma, J. C.; Dougherty, D. A. *Chem. Rev.* **1997**, *97*, 1303.
(2) Dougherty, D. A. *Science* **1996**, *271*, 163.
(3) Sunner, J.; Nishizawa, K.; Kebarle, P. *J. Phys. Chem.* **1981**, *85*, 1814.
(4) DeVos, A. M.; Ultsch, M.; Kossiakoff, A. A. *Science* **1992**, *255*, 306.
(5) Karlin, A. *Curr. Opin. Neurobiol.* **1993**, *3*, 299.
(6) Raves, M. L.; Harel, M.; Pang, Y. P.; Silman, I.; Kozikowski, A. P.; Sussman, J. L. *Nat. Struct. Biol.* **1997**, *4*, 57.
(7) Stauffer, D. A.; Karlin, A. *Biochemistry* **1994**, *33*, 6840.
(8) Mitchell, J. B.; Nandi, C. L.; McDonald, I. K.; Thornton, J. M.; Price, S. L. *J. Mol. Biol.* **1994**, *239*, 315.
(9) Zhong, W.; Gallivan, J. P.; Zhang, Y.; Li, L.; Lester, H. A.; Dougherty, D. A. *Proc. Natl. Acad. Sci. U.S.A.* **1998**, *95*, 12088.
(10) Donini, O.; Weaver, D. F. *J. Comput. Chem.* **1998**, *19*, 1515.
(11) Burley, S. K.; Petsko, G. A. *FEBS Lett.* **1986**, *203*, 139.
(12) Gallivan, J. P.; Dougherty, D. A. *Proc. Natl. Acad. Sci. U.S.A.* **1999**, *96*, 9459.
(13) Gokel, G. W.; De Wall, S. L.; Meadows, E. S. *Eur. J. Org. Chem.* **2000**, 2967.
(14) *Principles of Bioinorganic Chemistry*; Lippard, S. J., Berg, J. M., Eds.; University Science Books: Mill Valley, CA, 1994.
(15) Caldwell, J. W.; Kollman, P. A. *J. Am. Chem. Soc.* **1995**, *117*, 4177.
(16) Woodin, R. L.; Beauchamp, J. L. *J. Am. Chem. Soc.* **1978**, *100*, 501.
(17) Taft, R. W.; Anvia, F.; Gal, J.-F.; Walsh, S.; Capon, M.; Holmes, M. C.; Hosn, K.; Oloumi, G.; Vasanwala, R.; Yazdani, S. *Pure Appl. Chem.* **1990**, *62*, 17.
(18) Guo, B. C.; Purnell, J. W.; Castleman, A. W., Jr. *Chem. Phys. Lett.* **1990**, *168*, 155.
(19) Armentrout, P. B.; Rodgers, M. T. *J. Phys. Chem. A* **2000**, *104*, 2238.
(20) Amicangelo, J. C.; Armentrout, P. B. *J. Phys. Chem. A* **2000**, *104*, 11420.
(21) Gapeev, A.; Yang, C.-Y.; Klippenstein, S. J.; Dunbar, R. C. *J. Phys. Chem. A* **2000**, *104*, 3246.
(22) Huang, H.; Rodgers, M. T. *J. Phys. Chem. A* **2002**, *106*, 4277.
(23) Ryzhov, V.; Dunbar, R. C. *J. Am. Chem. Soc.* **1999**, *121*, 2259.
(24) Amunugama, R.; Rodgers, M. T. *J. Phys. Chem. A* **2002**, *106*, 5529.
(25) Ryzhov, V.; Dunbar, R. C.; Cerda, B.; Wesdemiotis, C. *J. Am. Soc. Mass Spectrom.* **2000**, *11*, 1037.
(26) Gapeev, A.; Dunbar, R. C. *J. Am. Chem. Soc.* **2001**, *123*, 8360.
(27) Feller, D.; Dixon, D. A.; Nicholas, J. B. *J. Phys. Chem. A* **2000**, *104*, 11414.
(28) Tsuzuki, S.; Yoshida, M.; Uchimaru, T.; Mikami, M. *J. Phys. Chem. A* **2001**, *105*, 769.
(29) Kim, C. Y.; Pooja, C. P.; Jain, A.; Christianson, D. W. *J. Am. Chem. Soc.* **2001**, *123*, 9620.
(30) http://www.prescriptionconsultation.com/anthrax.php3
(31) Mecozzi, S.; West, A. P., Jr.; Dougherty, D. A. *J. Am. Chem. Soc.* **1996**, *118*, 2307.
(32) Ryzhov, V.; Yang, C.-N.; Klippenstein, S. J.; Dunbar, R. C. *Int. J. Mass Spectrom.* **1999**, *185/186/187*, 913.
(33) Schroeter, K.; Wesendrup, R.; Schwarz, H. *Eur. J. Org. Chem.* **1998**, 565.
(34) Schröder, D.; Schroeter, K.; Schwarz, H. *Int. J. Mass Spectrom.* **2001**, *212*, 327.
(35) Ho, Y.-P.; Dunbar, R. C. *Int. J. Mass Spectrom.* **1999**, *182/183*, 175.
(36) Rodgers, M. T.; Armentrout, P. B. *J. Phys. Chem. A* **1997**, *101*, 1238.

(37) Rodgers, M. T.; Armentrout, P. B. *J. Phys. Chem. A* **1997**, *101*, 2614.
(38) Rodgers, M. T.; Armentrout, P. B. *J. Phys. Chem. A* **1999**, *103*, 4955.
(39) Rodgers, M. T.; Armentrout, P. B. *J. Chem. Phys.* **1998**, *109*, 1787.
(40) Rodgers, M. T.; Ervin, K. M.; Armentrout, P. B. *J. Chem. Phys.* **1997**, *106*, 4499.
(41) Rodgers, M. T.; Armentrout, P. B. *Int. J. Mass Spectrom.* **1999**, *185/186/187*, 359.
(42) Amunugama, R.; Rodgers, M. T. *Int. J. Mass Spectrom*. **2000**, *195/196*, 439.
(43) Rodgers, M. T.; Armentrout, P. B. *J. Am. Chem. Soc.* **2000**, *122*, 8548.
(44) Rodgers, M. T.; Stanley, J. R.; Amunugama, R. *J. Am. Chem. Soc*. **2000**, *122*, 10969.
(45) Rodgers, M. T. *J. Phys. Chem. A* **2001**, *105*, 2374.
(46) Amunugama, R.; Rodgers, M. T. *J. Phys. Chem. A* **2001**, *105*, 9883.
(47) Rodgers, M. T. *J. Phys. Chem. A* **2001**, *105*, 8145.
(48) Rodgers, M. T.; Armentrout, P. B. *J. Am. Chem. Soc*. **2002**, *124*, 2678.
(49) Valina, A. B.; Amunugama, R.; Huang, H.; Rodgers, M. T. *J. Phys. Chem. A* **2001**, *105*, 11057.
(50) Vitale, G.; Valina, A. B.; Huang, H.; Amunugama, R.; Rodgers, M. T. *J. Phys. Chem. A* **2001**, *105*, 11351.
(51) Chu, Y.; Yang, Z.; Rodgers, M. T. *J. Am. Soc. Mass Spectrom.* **2002**, *13*, 453.
(52) *Handbook of Chemistry and Physics*; Weast, R. C., Astle, M. J., Eds.; CRC Press: Boca Raton, FL, 1982; p E-61.
(53) Miller, K. J. *J. Am. Chem. Soc.* **1990**, *112*, 8533.
(54) (a) Teloy, E.; Gerlich, D. *Chem. Phys.* **1974**, *4*, 417. (b) Gerlich, D., Diplomarbeit, University of Freiburg, Federal Republic of Germany, 1971. (c) Gerlich, D. In *State-Selected and State-to-State Ion−Molecule Reaction Dynamics, Part I, Experiment*; Ng, C.-Y., Baer, M., Eds.; *Adv. Chem. Phys*. **1992**, *82*, 1.
(55) Dalleska, N. F.; Honma, K.; Armentrout, P. B. *J. Am. Chem. Soc.* **1993**, *115*, 12125.
(56) Aristov, N.; Armentrout, P. B. *J. Phys. Chem*. **1986**, *90*, 5135.
(57) Hales, D. A.; Armentrout, P. B. *J. Cluster Sci.* **1990**, *1*, 127.
(58) Ervin, K. M.; Armentrout, P. B. *J. Chem. Phys*. **1985**, *83*, 166.
(59) Dalleska, N. F.; Honma, K.; Sunderlin, L. S.; Armentrout, P. B. *J. Am. Chem. Soc*. **1994**, *116*, 3519.
(60) (a) Beyer, T. S.; Swinehart, D. F. *Commun. ACM* **1973**, *16*, 379. (b) Stein, S. E.; Rabinovitch, B. S. *J. Chem. Phys.* **1973**, *58*, 2438; *Chem. Phys. Lett.* **1977**, *49*, 1883.
(61) (a) Pople, J. A.; Schlegel, H. B.; Ragavachari, K.; DeFrees, D. J.; Binkley, J. F.; Frisch, M. J.; Whitesides, R. F.; Hout, R. F.; Hehre, W. J. *Int. J. Quantum Chem. Symp.* **1981**, *15*, 269. (b) DeFrees, D. J.; McLean, A. D. *J. Chem. Phys.* **1985**, *82*, 333.
(62) Khan, F. A.; Clemmer, D. C.; Schultz, R. H.; Armentrout, P. B. *J. Phys. Chem*. **1993**, *97*, 7978.
(63) Waage, E. V.; Rabinovitch, B. S. *Chem. Rev.* **1970**, *70*, 377.
(64) Chesnavich, W. J.; Bowers, M. T. *J. Phys. Chem.* **1979**, *83*, 900.
(65) Schultz, R. H.; Crellin, K. C.; Armentrout, P. B. *J. Am. Chem. Soc.* **1991**, *113*, 8590.
(66) More, M. B.; Glendening, E. D.; Armentrout, P. B. *J. Phys. Chem.* **1996**, *100*, 1605.
(67) Ray, D.; Feller, D.; More, M. B.; Glendening, E. D.; Armentrout, P. B. *J. Phys. Chem.* **1996**, *100*, 16116.
(68) Meyer, F.; Khan, F. A.; Armentrout, P. B. *J. Am. Chem. Soc.* **1995**, *117*, 9740.
(69) See, for example, Figure 1 in Dalleska et al.[55]
(70) Armentrout, P. B.; Simons, J. *J. Am. Chem. Soc.* **1992**, *114*, 8627.
(71) Frisch, M. J.; Trucks, G. W.; Schlegel, H. B.; Scuseria, G. E.; Robb, M. A.; Cheeseman, J. R.; Zakrzewski, V. G.; Montgomery, J. A., Jr.; Stratmann, R. E.; Burant, J. C.; Dapprich, S.; Millam, J. M.; Daniels, A. D.; Kudin, K. N.; Strain, M. C.; Farkas, O.; Tomasi, J.; Barone, V.; Cossi, M.; Cammi, R.; Mennucci, B.; Pomelli, C.; Adamo, C.; Clifford, S.; Ochterski, J.; Petersson, G. A.; Ayala, P. Y.; Cui, Q.; Morokuma, K.; Malick, D. K.; Rabuck, A. D.; Raghavachari, K.; Foresman, J. B.; Cioslowski, J.; Ortiz, J. V.; Stefanov, B. B.; Liu, G.; Liashenko, A.; Piskorz, P.; Komaromi, I.; Gomperts, R.; Martin, R. L.; Fox, D. J.; Keith, T.; Al-Laham, M. A.; Peng, C. Y.; Nanayakkara, A.; Gonzalez, C. Challacombe, M.; Gill, P. M. W.; Johnson, B.; Chen, W. Wong, M. W.; Andres, J. L.; Gonzales, C.; Head-Gordon, M.; Replogle, E. S.; Pople, J. A. *Gaussian 98*, Revision A.9; Gaussian, Inc.: Pittsburgh, PA, 1998.
(72) Becke, A. D. *J. Chem. Phys*. **1993**, *98*, 5648.
(73) Lee, C.; Yang, W.; Parr, R. G. *Phys. Rev. B* **1988**, *37*, 785.
(74) The Hay−Wadt valence basis sets and effective core potentials were obtained from the Extensible Computational Chemistry Environment Basis Set Database (available on the Internet at http://www.emsl.pnl.gov:2080/forms/basisform.html), as developed and distributed by the Molecular Science Computing Facility, Environmental and Molecular Sciences Laboratory, which is part of the Pacific Northwest National Laboratory, P.O. Box 999, Richland, WA 99352, and funded by the U.S. Department of Energy. For the original valence basis set and ECP reference, see Hay, P. J.; Wadt, W. R. *J. Chem. Phys.* **1985**, *82*, 299.
(75) Glendening, E. D.; Feller, D.; Thompson, M. A. *J. Am. Chem. Soc.* **1994**, *116*, 10657.
(76) Walter, D.; Armentrout, P. B. *J. Am. Chem. Soc*. **1998**, *120*, 3176.
(77) Foresman, J. B.; Frisch, Æ. *Exploring Chemistry with Electronic Structure Methods*, 2nd ed.; Gaussian: Pittsburgh, PA, 1996; p 64.
(78) Boys, S. F.; Bernardi, R. *Mol. Phys.* **1979**, *19*, 553.
(79) Van Duijneveldt, F. B.; van Duijneveldt-van de Rijt, J. G. C. M.; van Lenthe, J. H. *Chem. Rev.* **1994**, *94*, 1873.
(80) Dzidic, I.; Kebarle, P. *J. Phys. Chem*. **1970**, *74*, 1466.
(81) Davidson, W. R.; Kebarle, P. *J. Am. Chem. Soc*. **1976**, *98*, 6125.
(82) Dalleska, N. F.; Tjelta, B. L.; Armentrout, P. B. *J. Phys. Chem*. **1994**, *98*, 4191.
(83) Feller, D.; Glendening, E. D.; Kendall, R. A.; Peterson, K. A. *J. Chem. Phys*. **1994**, *100*, 49881.
(84) More, M. B.; Glendening, E. D.; Ray, D.; Feller, D. Armentrout, P. B. *J. Phys. Chem.* **1996**, *100*, 1605.
(85) More, M. B.; Ray, D.; Armentrout, P. B. *J. Phys. Chem. A* **1997**, *101*, 1238.
(86) More, M. B.; Ray, D.; Armentrout, P. B. *J. Phys. Chem. A* **1997**, *101*, 4254.
(87) More, M. B.; Ray, D.; Armentrout, P. B. *J. Phys. Chem. A* **1997**, *101*, 7007.
(88) Lifshitz, C. *Adv. Mass Spectrom.* **1989**, *11*, 113.
(89) The metal ring−centroid distance is defined as the distance from the metal atom to the central point within the aromatic ring that is in the plane of the carbon atoms.
(90) Wilson, R. G.; Brewer, G. R. *Ion Beams: With Applications to Ion Implantation*; Wiley: New York, 1973; pp 118−124.